AMSE JOURNALS-AMSE IIETA publication-2017-Series: Modelling B; Vol. 86; N°1; pp 126-140
Submitted Jan. 2017; Revised March 15, 2017, Accepted April 15, 2017
https://doi.org/10.18280/mmc_b.860110

Numerical Analysis of Solid-Liquid Turbulent Flow in Francis Turbine Spiral Case

* Huiyan Wang, ** Xiaobing Liu

* Key Laboratory of Fluid and Power Machinery (Xihua University), Ministry of Education
Chengdu610039 China, (why@mail.xhu.edu.cn)
** School of Energy and Power Engineering, Xihua University
Chengdu, 610039 China, (corresponding author: liuxb@mail.xhu.edu.cn)

Abstract

Based on the hydrological conditions of a hydropower station, the three-dimensional turbulent flow in a Francis turbine with splitter blades was numerically simulated in sandy water. The solid-liquid two-phase turbulent flow in the spiral case at different loads was numerically analyzed in emphasis, including the distribution of pressure, sand volume and velocity on different sections of the spiral case. The movement pattern of sandy water in the turbine spiral case was studied. The results show that the pressure distribution in the spiral case varies uniformly at different loads, a high pressure zone will be generated at the bottom of the spiral case and a low pressure zone at the outlet; the spiral case bottom and the nose has the largest area of sand and the highest sand volume fraction; with the increasing of the load, the high pressure zone moves from the bottom to the exterior margin, the sand volume fraction decreases, and the sediment-carrying capacity increases. At off-design conditions, the joint effect of sand abrasion and cavitation will worsen the erosion of the spiral case.

Key words

Francis turbine, spiral case, solid-liquid two-phase turbulent flow, sand volume fraction, pressure distribution

1. Introduction

Silt erosion in Francis turbines is a very serious problem and has caused huge losses to the hydropower industry. The process of erosion damage is influenced by a number of factors, namely, the average velocity of particles, mass of particles, concentration of abrasive particles in fluid, size distribution of particles, and their average grain size, angle of impingement, time interval of the attack and the erosion resistance of structural material [1]. The flow in a turbine in sediment-laden river is multi-phase flow. The complexity of the internal flow has been studied by many scholars.

With the development of numerical methods [2-5] and experimental technologies in recent years, many experts and scholars have studied the solid-liquid two-phase flow in turbines and obtained some achievements. The influence of turbine performance by sediment concentration was analyzed in sandy water. Liu, et al. numerically simulated the trajectory of sediment particles in the three dimensional flow field in a turbine [6], and discussed the flow and hydraulic loss in the turbine in sediment-laden flow and analyzed the sediment erosion of the turbine [7]. Takagi, et al. reported the hydraulic performance tests on a Francis turbine model with sediment laden flow in Japan, and showed that the turbine's best efficiency decreased in direct proportion to the increase in solids concentration [8]. Thapa, et al. optimized the turbine working in sediment-laden flow through numerical simulation and experimental study which effectively reduces the sediment erosion and improves the turbine efficiency [9]. Zhang, et al. analyzed the two-phase flow mechanism in the flow components of a turbine and predicted the performance of a Francis turbine operating in sandy river [10]. L. Weili, et al. studied the cavitation erosion characteristics of axial-flow turbine in sediment-laden flow, and obtained the conclusion that turbine is more prone to cavitate in sediment-laden flow than in clear water [11]. Peng, et al. simulated the liquid-solid two-phase flow in Francis turbines, and predicted the abrasion characteristics on the runner blades and guide vanes with sediment flow [12]. The CFD software was used and secondly developed to simulate the solid-liquid two-phase flow in turbines. Tang, et al. conducted secondary development to CFD, and studied the solid-liquid two-phase flow in a Francis turbine by using the improved algebraic model, and the simulated results are consistent with the actual project [13]. The joint effect of sand wear and cavitation to the erosion of turbine components was studied. Li and Carpenter found out that the flow surface of hydraulic machinery will be damaged by the joint action of cavitation erosion and abrasion during the cavitation process in sediment-laden flow, which is a failure mode different from cavitation erosion or abrasion, and the level of destruction is much serious than that of single effect [14]. Li, et al. analyzed the inner flow field of volute, explored and predicted the law of wear and cavitation [15]. Thapa, et al.

used the rotating disc apparatus (RDA) to study the synergistic effect of sediment erosion and cavitation in hydraulic turbine components and turbine materials [16]. Wang, studied the influence of solid volume fractions on the performance of Francis turbines, and found that the joint effect of cavitation and sand erosion will be aggravated with the increasing of solid volume fractions [17]. Eltvik et al. investigated the relationships between the sediment erosion and operating conditions of the turbine, and found that the erosion process is strongly dependent on the operating conditions of the turbine [18].

However, the effects of operating conditions on the solid-liquid two-phase flow in the spiral case are seldom studied. In this paper, the solid-liquid two-phase flow in a turbine spiral case as affected by the operating conditions was numerically simulated in sandy river, the flow pattern in the spiral case was analyzed and studied, and the sand erosion was numerically predicated.

2. Mathematical Model

The following assumptions have been made in this study:

- The liquid phase (water) is incompressible. The solid phase (sand) is continuous. The physical properties of each phase are constants.
- The solid phase consists of sand particles spherical in shape and uniform in size.
- Neither the suspended matter nor the carrier liquid undergoes any phase change.
- Interactions between particles, as well as between particles and the wall are neglected.

2.1 Basic Equations of Solid-Liquid Two-Phase Flow

The motion equations of solid-liquid two-phase flow in the Eulerian coordinate system are as follows [19]:

Liquid phase continuity equation:

$$\frac{\partial \phi_L}{\partial t} + \frac{\partial}{\partial x_i}(\phi_L U_i) = 0 \tag{1}$$

Solid phase continuity equation:

$$\frac{\partial \phi_S}{\partial t} + \frac{\partial}{\partial x_i}(\phi_S V_i) = 0 \tag{2}$$

Liquid phase momentum equation:

$$\frac{\partial}{\partial x_i}(\phi_L U_i)+\frac{\partial}{\partial x_k}(\phi_L U_i U_k)=-\frac{1}{\rho_L}\phi_L\frac{\partial P}{\partial x_i}+\nu_L\frac{\partial}{\partial x_i}[\phi_L(\frac{\partial U_i}{\partial x_k}+\frac{\partial U_k}{\partial x_i})]-\frac{B}{\rho_L}\phi_L\phi_S(U_i-V_i)+\phi_L g_i \quad (3)$$

Solid phase momentum equation:

$$\frac{\partial}{\partial t}(\phi_S V_i)+\frac{\partial}{\partial x_k}(\phi_S V_i V_k)=-\frac{1}{\rho_S}\phi_S\frac{\partial P}{\partial x_i}+\nu_S\frac{\partial}{\partial x_k}[\phi_S(\frac{\partial V_i}{\partial x_k}+\frac{\partial V_k}{\partial x_i})]-\frac{B}{\rho_S}\phi_L\phi_S(V_i-U_i)+\phi_S g_i \quad (4)$$

Where, Φ is a phase volume number, $\Phi_L+\Phi_S=1$, and the subscripts L and S represent the liquid and solid phases, respectively; U_i and V_i are respectively the velocity components of the liquid and solid phases; t is the time; x is the coordinate component, and the subscripts i and k are the tensor coordinates; ρ is the material density of phases; v is the kinematic viscosity coefficient; P represents the gravity acceleration component; g is the component of gravity acceleration; B represents the interaction coefficient between phases, $B=18(1+B_0)\rho_L\nu_L/d^2$, where d is the particle diameter. The introduction of B_0 in it is to consider other factors besides the stokes linear resistance. Generally speaking, B_0 is not a constant, for it is related to flow field parameters such as the particle Reynolds number.

2.2 Turbulence Calculation Model

The Standard k-ε model was used in this study, which can be written as:

$$\frac{\partial}{\partial t}(\rho k)+\frac{\partial}{\partial x_i}(\rho k u_i)=\frac{\partial}{\partial x_j}\left[\left(\mu+\frac{\mu_t}{\sigma_k}\right)\frac{\partial k}{\partial x_j}\right]+G_k+G_b-\rho\varepsilon-Y_M+S_k \quad (5)$$

$$\frac{\partial}{\partial t}(\rho\varepsilon)+\frac{\partial}{\partial x_i}(\rho\varepsilon u_i)=\frac{\partial}{\partial x_i}\left[\left(\mu+\frac{\mu_t}{\sigma_\varepsilon}\right)\frac{\partial\varepsilon}{\partial x_j}\right]+C_{1\varepsilon}\frac{\varepsilon}{k}(G_k+C_{3\varepsilon}G_b)-C_{2\varepsilon}\rho\frac{\varepsilon^2}{k}+S_\varepsilon \quad (6)$$

Where, k is the turbulent kinetic energy; ε is the energy dissipation rate; u_i is the mean velocity; μ_t is the turbulent viscosity; G_k is the turbulent kinetic energy caused by the average velocity gradient; G_b represents the turbulent kinetic energy caused by buoyancy influence; Y_M represents the influence of the total dissipation rate by the compressible turbulence fluctuation expansion; σ_k and σ_ε are the reciprocals of effective turbulent Prandtl numbers of the turbulent kinetic energy k and dissipation rate ε; $C_{1\varepsilon}$ = 1.44, $C_{2\varepsilon}$ = 1.92, $C_{3\varepsilon}$ = 0.09 are default constants; and S_k and S_ε are the User-defined source terms.

This model has been used to simulate the solid-liquid two-phase turbulent flow in the runner of Francis turbines used in Jinping II Hydropower Station on Yalong River in China, and has been proved reliable [20].

3. Calculation Parameters

3.1 Basic Parameters of the Turbine

The Francis turbine with splitter blades in Jinping II Hydropower Station on Yalong River in China was selected, and the entire flow passage of this turbine was numerically simulated. The turbine in this station is a vertical shaft Francis turbine, and the design parameters of the turbine are listed in Table 1.

Table 1. Design parameters of the turbine

Parameters	Value
Design head, H_d	288m
Design flow rate, Q_d	228.6 m^3/s
Design output, N_d	610 MW
Design speed, n_d	166.7 r/min
Specific speed, N_S	110
Runner inlet diameter, D_1	6557 mm
Runner outlet diameter, D_2	4600 mm
Number of long runner blades, Z'	15
Number of short runner blades, Z''	15
Number of stay vanes, Z_2	23
Number of wicket gates, Z_1	24

On the basis of UG software platform [21], the digital geometry modeling of all flow components was completed by using the data provided by the power station. The three dimensional model of the spiral case is shown in Fig.1. And then, the CFD dedicated preprocessor Gambit software was used to generate unstructured meshes of various flow components, and the number of meshes in the whole flow passage is 2,193,457 which can meet the independency requirement of less than 5%. The mesh diagram of the spiral case is shown in Fig.2.

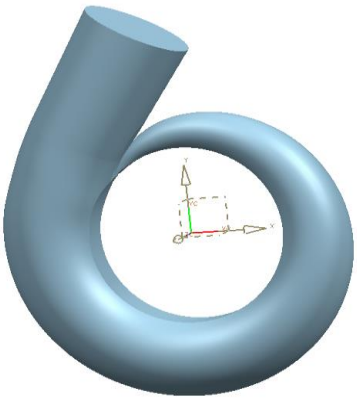

Fig.1. Three dimensional model of the spiral case

Fig.2. Meshes of the spiral case

3.2 Calculation Parameters

Three conditions were selected according to the design parameters of the turbine and the scope of its operating conditions. The volume fractions of sand in various conditions are listed in Table 2. The particle sizes were provided by the power station, and the average particle diameter was taken as 0.246mm.

Table 2. Statistics of CFD calculation conditions

Condition	Loading situation	Guide vane opening (°)	Flow rate (m^3/s)	Sand volume fraction (%)
1	1/4	7.3	66.0	1.519
2	1/2	12.5	117.0	1.85
3	1/1	24	228.6	1.985

3.3 Boundary Conditions

The SIMPLE algorithm of standard k-ε model was adopted. The velocity inlet was used as the inlet boundary conditions. The inlet velocity was determined according to the flow rate. Assuming the incoming flow at the inlet is uniform and the inlet velocity is perpendicular to the inlet boundary surface, the inlet velocities at various conditions can be calculated by using the data in Table 2. For the outlet boundary conditions, the pressure outlet was determined according to the suction height, its direction was perpendicular to the outlet surface, and the outlet section pressure was calculated as 99,081 Pa. The velocity on the solid wall can meet the no-slip wall condition, and the standard wall function was adopted for the near-wall area. While determining

the velocity and pressure of the inlet and outlet, the volume fraction and particle size of sand were also provided.

4. Calculation Results and Analysis

According to the calculation parameters and by using the Fluent software and the established numerical simulation model of solid-liquid two-phase turbulent flow, the two-phase flow in the spiral case under three different load conditions were numerically simulated to obtain the distributions of pressure, sand volume and velocity vector at different sections of the spiral case.

4.1 Condition 1

In condition 1, the unit load is 1/4 of the rated load, the wicket gate opening is 7.3°, and the flow rate is 66.0 m^3/s. The distributions of pressure, sand volume fraction and velocity vector on several sections of the spiral case were calculated, as shown from Fig.3.a to Fig.3.h.

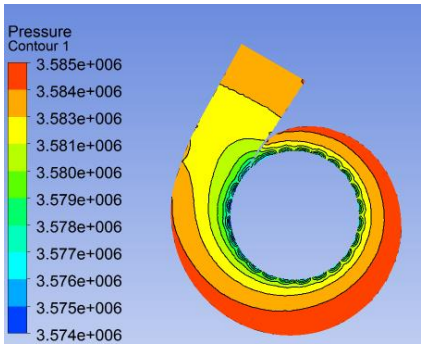

a. Pressure distribution on section x-y

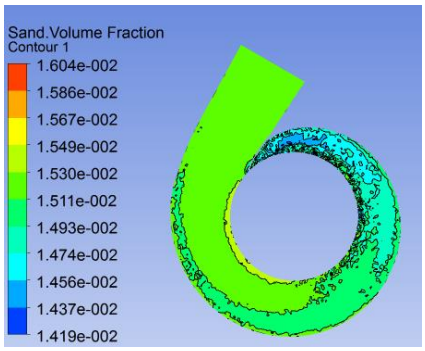

b. Sand volume fraction on section x-y

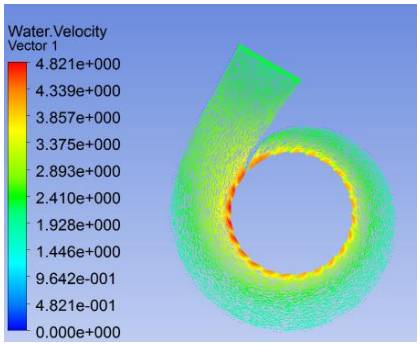

c. Velocity vector distribution of water on section x-y

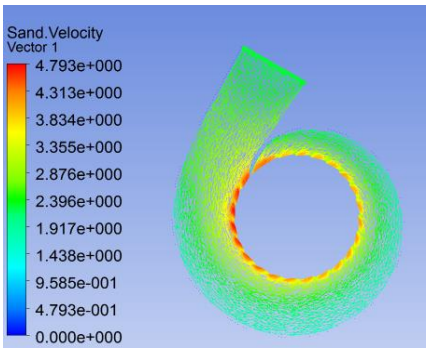

d. Velocity vector distribution of sand on section x-y

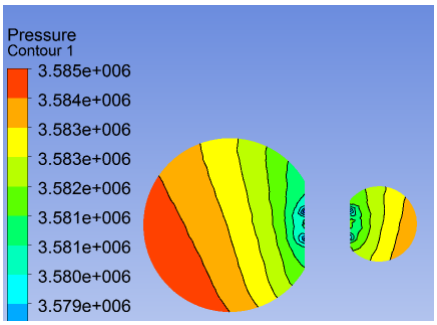

e. Pressure distribution on section y-z

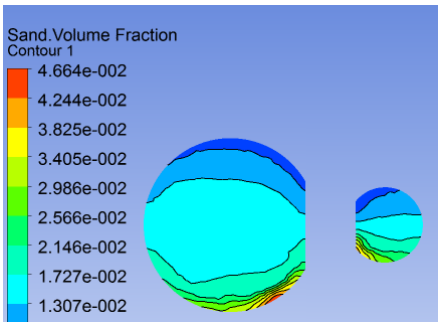

f. Sand volume fraction on section y-z

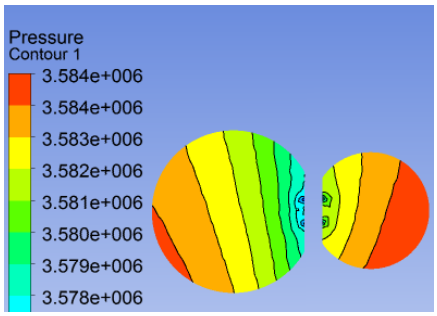

g. Pressure distribution on section x-z

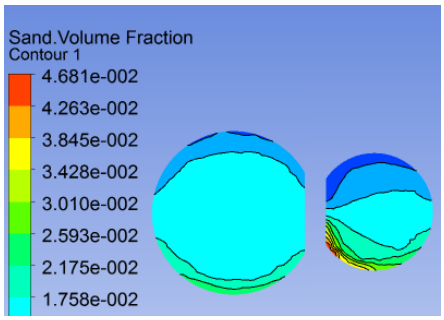

h. Sand volume fraction on section x-z

Fig.3. Distributions of pressure, sand volume fraction and velocity vector on different sections of the spiral case in condition 1

It can be known from Fig.3.a to Fig.3.h that when the load of the unit is 1/4 (condition 1), the pressure distributions on various sections of the spiral case have a few differences and are basically changing uniformly. The pressure is gradually reducing along the radial direction from the spiral case inlet to the outlet. It has good symmetry in circumferential direction and basically follows the cylindrical layer independence assumption. On sections y-z and x-z, the high pressure zone is mainly concentrated at the bottom of the spiral case closing to lateral area, and the low pressure zone is always at the spiral case outlet near the stay ring. The sand volume fractions on different sections of the spiral case are non-uniform. From the spiral case inlet to the outlet, the sand volume fraction has a general decreasing trend. The sand volume fraction on the upper part of the spiral case is low, while higher at the bottom near the stay ring, which indicates that the sand will settle down at the bottom of the spiral case. In this condition, the flow rate is small, so does the sediment-carrying capacity. Due to gravity, sand will settle down at the bottom of the spiral case very easily. On section x-y, the velocity vector distributions of water and sand are roughly uniform. The velocity is gradually increasing from the inlet to the outlet along the circumferential direction, and the velocity near the nose is high. The velocity has a trend of

gradual decreasing along the flow direction in the spiral case. The velocity vector distributions of water and sand are basically consistent.

4.2 Condition 2

In condition 2, the unit load is 1/2 of the rated load, the wicket gate opening is 12.5°, and the flow rate is 117.0 m^3/s. The distributions of pressure, sand volume fraction and velocity vector on several sections of the spiral case were calculated, as shown from Fig.4.a to Fig.4.h.

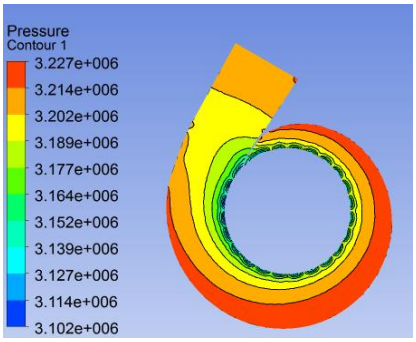

a. Pressure distribution on section x-y

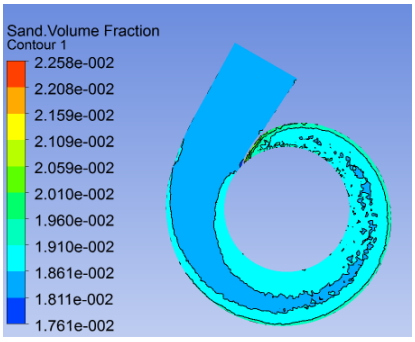

b. Sand volume fraction on section x-y

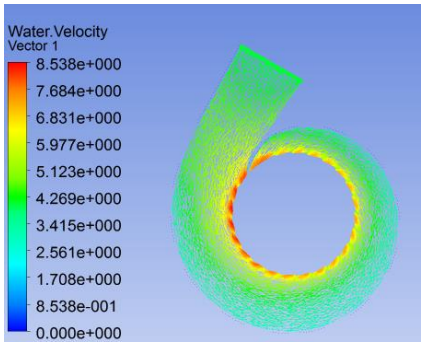

c. Velocity vector distribution of water on section x-y

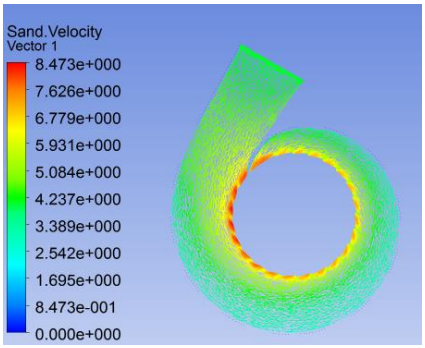

d. Velocity vector distribution of sand on section x-y

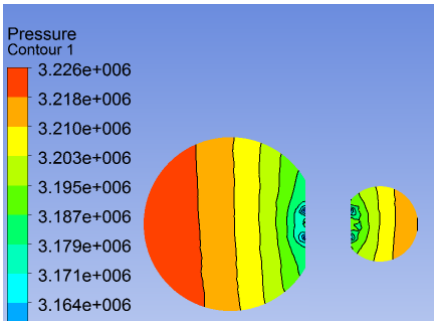

e. Pressure distribution on section y-z

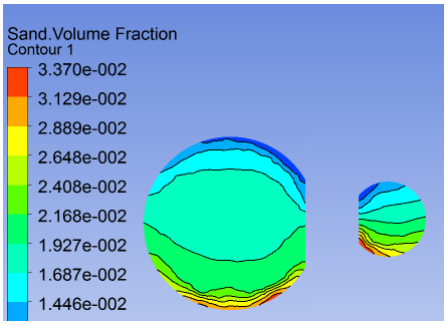

f. Sand volume fraction on section y-z

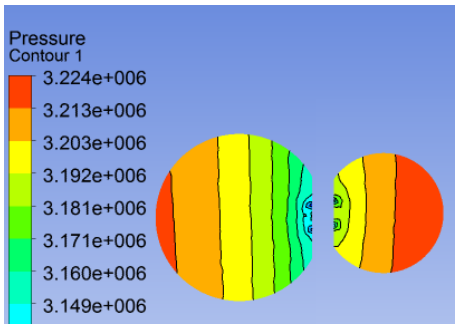

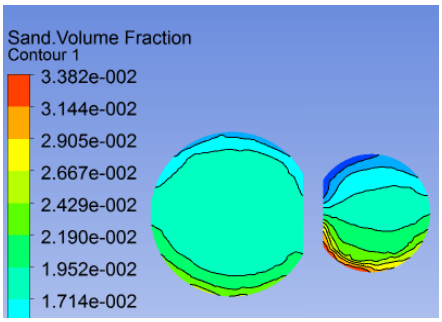

g. Pressure distribution on section x-z h. Sand volume fraction on section x-z

Fig.4. Distributions of pressure, sand volume fraction and velocity vector on different sections of the spiral case in condition 2

It can be known from Fig.4.a to Fig.4.h that when the load of single unit is 1/2 (condition 2), the pressure distributions on various sections of the spiral case are not much different from condition 1, and the changes are uniform. The pressure is gradually reducing along the radial direction from the spiral case inlet to the outlet. It has good symmetry in circumferential direction and basically follows the cylindrical layer independence assumption. On sections y-z and x-z, the high pressure zone is mainly concentrated on the lateral of the spiral case, which is closer to the horizontal section than condition 1. The low pressure zone is mainly distributed at the spiral case outlet near the stay ring, which is basically consistent with condition 1. The sand volume fractions on different sections of the spiral case are less uniformly distributed. From the spiral case inlet to the outlet, the sand volume fraction has a general increasing trend, and the sand volume fraction at the nose is slightly high. The sand volume fraction on the upper part of the spiral case is low, while higher at the bottom near the stay ring, which indicates that the sand has a trend to settle down at the bottom of the spiral case. In this condition, the sand volume fraction is slightly lower than that of condition 1, while the distribution area of higher sand volume fraction is larger than that of condition 1. On section x-y, the velocity vector distributions of water and sand are roughly uniform. On the circumferential direction, the velocity is gradually increasing from the inlet to the outlet along the radial direction, and the velocity near the nose is high. The velocity has a trend of gradual decreasing along the flow direction into the spiral case, which is basically consistent with condition 1. The velocity vector distributions of water and sand are basically consistent with condition 1.

4.3 Condition 3

In condition 3, the unit is in full load, the wicket gate opening is 24°, and the flow rate is 228.6 m^3/s. The distributions of pressure, sand volume fraction and velocity vector on several sections of the spiral case were calculated, as shown from Fig.5.a to Fig.5.h.

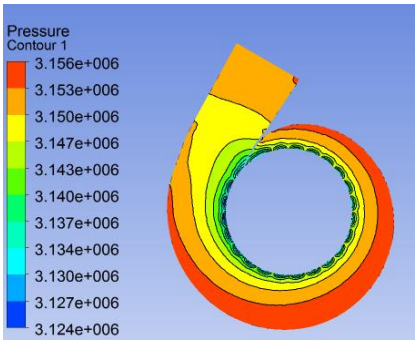

a. Pressure distribution on section x-y

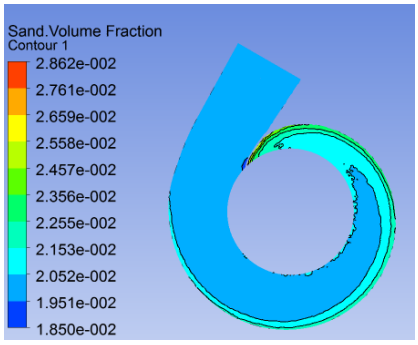

b. Sand volume fraction on section x-y

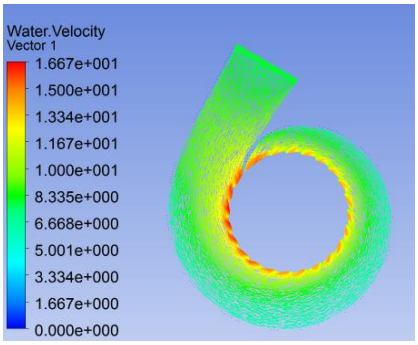

c. Velocity vector distribution of water on section x-y

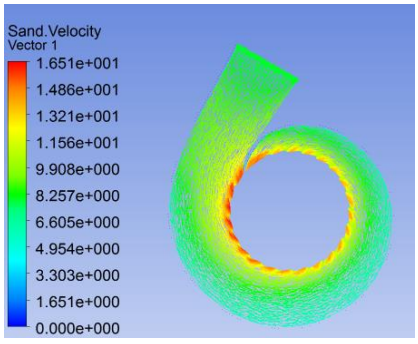

d. Velocity vector distribution of sand on section x-y

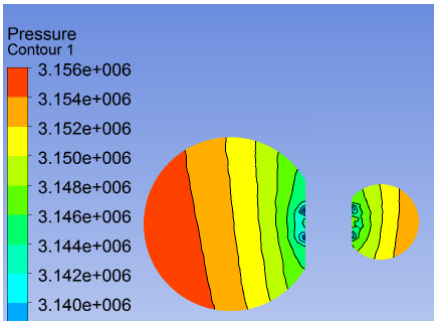

e. Pressure distribution on section y-z

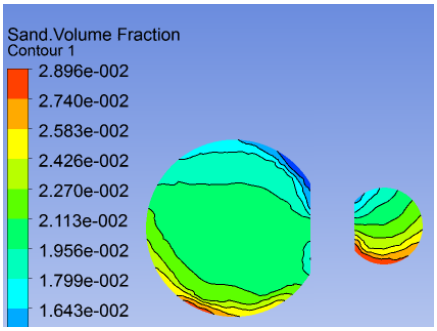

f. Sand volume fraction on section y-z

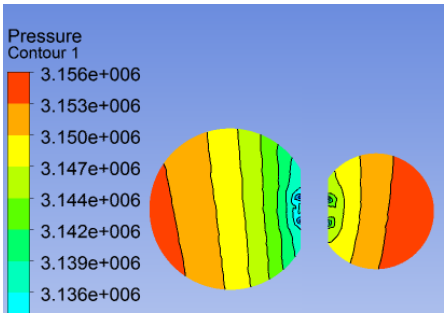

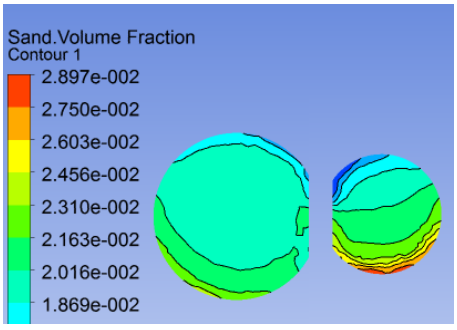

g. Pressure distribution on section x-z h. Sand volume fraction on section x-z

Fig.5. Distributions of pressure, sand volume fraction and velocity vector on different sections of the spiral case in condition 3

When the load of single unit is full (condition 3), the pressure distributions on various sections of the spiral case have a few differences, and the changes are basically uniform. The pressure is gradually reducing along the radial direction from the spiral case inlet to the outlet. It has good symmetry in circumferential direction and basically follows the cylindrical layer independence assumption. On sections y-z and x-z, the high pressure zone is mainly concentrated on the lateral of the spiral case, and the high pressure zone is more symmetrical than that in conditions 1 and 2. The low pressure zone is always at the spiral case outlet near the stay ring, which is consistent with that of conditions 1 and 2. The sand volume fractions on different sections of the spiral case are less uniformly distributed. From the spiral case inlet to the outlet, the sand volume fraction has a general increasing trend, and the sand volume fraction at the nose is high. The sand volume fraction at the bottom of the spiral case is also high, which indicates that the sand has a trend to settle down at the bottom of the spiral case. The sand volume fraction in condition 3 is lower than that of conditions 1 and 2, but the area of high sand volume fraction is larger than that of conditions 1 and 2. On section x-y, the velocity vector distributions of water and sand are roughly uniform. On the circumferential direction, the velocity is gradually increasing from the inlet to the outlet along the radial direction, and the velocity near the nose is high. The velocity has a trend of gradual decreasing along the flow direction into the spiral case, which is basically consistent with conditions 1 and 2. The velocity vector distributions of water and sand are basically consistent with conditions 1 and 2.

5. Conclusion

The following conclusions can be obtained through the analyses:

1) Under various conditions, the pressure distribution in the spiral case is changing uniformly. The pressure is gradually reducing along the radial direction from the spiral case inlet to the outlet in each condition, and basically follows the cylindrical layer independence assumption. There is a high pressure zone at the bottom of the spiral case close to the outer margin and a low pressure zone at the spiral case outlet near the stay ring. With the increasing of load, the high pressure zone gradually moves from the bottom to the horizontal exterior margin of the spiral case.

2) Under various conditions, the sand distribution area at the bottom of the spiral case and near the nose is large, and the sand volume fraction is high. Therefore, damages of the nose by sand can be quantitatively predicated under various conditions. The sand has a trend to settle down at the bottom of the spiral case. With the increasing of load, the sand volume fraction at the bottom decreases.

3) The sediment-carrying capacity increases with the flow rate. With the increasing of load, the guide vane opening increases, the sand volume fraction increases, and the velocity of sediment-laden flow accelerates, while the sand settled down at the bottom of the spiral case reduces. Sand will wear the flow components at any condition, especially in cavitation condition. If deviating from the design condition, the damages of the turbine by sediment-laden water will be intensified, and this will significantly affect the energy characteristics of the unit. The research results show that the lethal damage to the turbine is the joint action of sand abrasion and cavitation. These two factors promote each other all the time and accelerate the damages to the flow components, especially at off-design conditions. To guarantee the safety and stable operation of power station units, the power station shall operate to avoid the adverse conditions.

Acknowledgement

This work was funded by the Open Research Subject of Key Laboratory of Fluid and Power Machinery (Xihua University), Ministry of Education (Grant No. szjj2015-026).

References

1. C.G. Duan, V.Y. Karelin, Abrasive erosion and corrosion of hydraulic machinery, 2002, London: Imperial College Press, vol. 2.
2. M. Rashad, X. Zhang, H. Elsadek, Numerical simulation of two-phase flow modeling of solid propellant combustion, 2014, International Journal of Heat and Technology, vol. 32, no. 1-2, pp. 111-118.
3. H. Bounaouara, H. Ettouati, H. B. Ticha, et al., Numerical simulation of gas-particles two phase flow in pipe of complex geometry: Pneumatic conveying of olive cake particles toward a dust burner, 2015, International Journal of Heat and Technology, vol. 33, no. 1, pp. 99-106.

4. S. Lv, M. Feng, Three-dimensional numerical simulation of flow in Daliushu Reach of the Yellow River, 2015, International Journal of Heat and Technology, vol. 33, no. 1, pp. 107-114.
5. Q. Guo, X. Qi, Z. Wei, et al., 3D numerical simulation and analysis of refrigeration performance of the small diameter vortex tube, 2016, International Journal of Heat and Technology, vol. 34, no. 3, pp. 513-520.
6. X.B. Liu, J.C. Zhang, L.J. Cheng, Numerical simulation of sand particle motion in rotating field, 1998, Journal of Hydrodynamics. Ser. A, vol.13, no.3, pp. 338-346.
7. X.B. Liu, Numerical simulation of sediment abrasion in hydraulic machinery, 2000, Sichuan Univ Sci Technol, vol. 19, no. 2, pp. 79-84.
8. T. Takagi, T. Okamura, J. Sato, Hydraulic performance of a Francis-turbine for sediment-laden flow, 1988, Hitachi Review, vol. 37, no. 2, pp. 115-120.
9. B. Thapa, O.G. Dahlhaug, B.S. Thapa, K.P. Shrestha, Accelerated testing for resistance to sand erosion in hydraulic turbines, 2012, Fourth International Conference on Water Resources and Renewable Energy Development in Asia, 2012, Chiang Mai, Thailand, pp. 26-27.
10. H.K. Zhang, X.B. Liu, T. He, et al., Three-dimensional performance prediction of whole flow passage of Francis turbine operating in Sandy River, 2009, Water Resources and Power, vol. 27, no. 2, pp. 158-160.
11. L. Weili, L. Jinling, L. Xingqi, L. Yuan, Research on the cavitation characteristic of Kaplan turbine under sediment flow condition, 2010, IOP Conference Series: Earth and Environmental Science, vol. 12, no. 1, pp. 012022.
12. P. Guangjie, W. Zhengwei, X. Yexiang, L. Yongyao, Abrasion predictions for Francis turbines based on liquid-solid two-phase fluid simulations, 2013, Engineering Failure Analysis, vol. 33, pp. 327-335.
13. X.L. Tang, S.Y. Yang, F.J. Wang, Y.L. Wu, Numerical investigations of solid-liquid two-phase turbulent flows through Francis turbine, 2012, Advanced Materials Research, vol. 548, pp. 853-859.
14. S.C. Li, P.W. Carpenter, Anti erosion turbine: cavitation & silt synergetic erosion, 2002, The 9th International Symposium on Transport Phenomena and Dynamics of Rotating Machinery, 2002, Hawaii, USA, pp. 10-14.
15. Q.F. Li, R.N. Li, W. Han, et al., CFD simulation of sand-water two-phase inner flow field of volute, 2007, Drainage and Irrigation Machinery, vol. 25, no. 5, pp. 61-64.

16. B.S. Thapa, B. Thapa, O.G. Dahlhaug, Empirical modelling of sediment erosion in Francis turbines, 2012, Energy, vol. 41, no. 1, pp. 386-391.
17. H. Wang, Research on the Influence of Solid Volume Fractions on Turbine Performance, 2016, International Journal of Heat and Technology, vol. 34, no. 4, pp. 630–636.
18. M. Eltvik, Sediment Erosion in Francis Turbines, 2013, Doctoral thesis, Trondheim: Norwegian University of Science and Technology. URN: urn:nbn:no:ntnu:diva-22755
19. X.B. Liu, Solid-liquid two-phase flow and numerical simulation in turbo machinery. Beijing: China Water Conservancy and Hydropower Press, 1996.
20. H. Hua, Y. Z. Zeng, H. Y. Wang, et al., Numerical analysis of solid–liquid two-phase turbulent flow in Francis turbine runner with splitter blades in sandy water, 2015, Advances in Mechanical Engineering, vol. 7, no. 3, pp. 1-10.
21. Y. Yang, C. Zhang, Y. Huang, et al., UG8.0 in the simple application of automatic shoes-washing machine design, 2016, Mathematical Modelling of Engineering Problems, vol. 3, no. 2, pp. 59-62.
22. J.R Simson, L.R. John, A.B Jerry, Title of paper, 2008, Journals title, vol. 16, no. 1, pp. 67-75.
23. Jaime Gil, Title of paper, 2006, XXX conference, 2006, Barcelona, Spain, pp. 54-56.
24. Author, Title of article, www.xxx.org, access date March 2012
25. J.R. Simson, High performance digital music synthesizer, 1992, IEEE Trans. on Consum. Electron, vol. 38, no. 2, pp. 85-90.